Nanobody repertoire generated against the spike protein of ancestral SARS-CoV-2 remains efficacious against the rapidly evolving virus

Natalia E. Ketaren[1,#], Fred D. Mast[2,#], Peter C. Fridy[1,#], Jean Paul Olivier[2,#], Tanmoy Sanyal[3,#], Andrej Sali[3], Brian T. Chait[4,*], Michael P. Rout[1,*]John D. Aitchison[2,5,6,*]

1. Laboratory of Cellular and Structural Biology, The Rockefeller University, New York, New York 10065, 12 USA

2. Center for Global Infectious Disease Research, Seattle Children's Research Institute, Seattle, 10 Washington 98109, USA.

3. Department of Bioengineering and Therapeutic Sciences, Department of Pharmaceutical Chemistry, 17 California Institute for Quantitative Biosciences, Byers Hall, 1700 4th Street, Suite 503B, University of California, San Francisco, San Francisco, California 94143, USA.

4. Laboratory of Mass Spectrometry and Gaseous Ion Chemistry, The Rockefeller University, New York, 14 New York 10065, USA

5. Department of Pediatrics, University of Washington, Seattle, Washington 98195, USA.

6. Department of Biochemistry, University of Washington, Seattle, Washington 98195, USA.

Author Footnotes
# These authors contributed equally
*Correspondence:
john.aitchison@seattlechildrens.org
chait@rockefeller.edu
rout@rockefeller.edu

Abstract

To date, all major modes of monoclonal antibody therapy targeting SARS-CoV-2 have lost significant efficacy against the latest circulating variants. As SARS-CoV-2 omicron sublineages account for over 90% of COVID-19 infections, evasion of immune responses generated by vaccination or exposure to previous variants poses a significant challenge. A compelling new therapeutic strategy against SARS-CoV-2 is that of single domain antibodies, termed nanobodies, which address certain limitations of monoclonal antibodies. Here we demonstrate that our high-affinity nanobody repertoire, generated against wild-type SARS-CoV-2 spike protein (Mast, Fridy et al. 2021), remains effective against variants of concern, including omicron BA.4/BA.5; a subset is predicted to counter resistance in

emerging XBB and BQ.1.1 sublineages. Furthermore, we reveal the synergistic potential of nanobody cocktails in neutralizing emerging variants. Our study highlights the power of nanobody technology as a versatile therapeutic and diagnostic tool to combat rapidly evolving infectious diseases such as SARS-CoV-2.

Introduction

SARS-CoV-2 has infected >40% of the world's population (Collaborators 2022) resulting in a devastating loss of life. As the SARS-CoV-2 pandemic enters its endemic phase (Meng, Irwin et al. 2023, Pilz and Ioannidis 2023), multiple new variants continue to circulate. Since its initial spread, the rapid adaptation of the virus to selective pressures continues to produce variants of concern (VoC), of which the omicron variants presently account for over 90% of current SARS-CoV-2 infections (www.cdc.gov). SARS-CoV-2 displays three structural proteins that are potential targets for therapeutic intervention, but the primary focal point of vaccine development and many therapeutic strategies is the spike surface glycoprotein, which the virus uses to gain cell entry by attaching to the host cell angiotensin-converting enzyme 2 (ACE2) receptor (Jackson, Anderson et al. 2020, Krammer 2020, Letko, Marzi et al. 2020, Polack, Thomas et al. 2020). The spike protein trimer consists of three domains: the receptor binding domain (RBD) on S1 that binds ACE2, the S1 N-terminal domain (NTD) that has a poorly defined function, and the S2 domain that is involved in virus-host cell membrane fusion (Walls, Park et al. 2020, Jackson, Farzan et al. 2022). Glycosylation is most extensive on the NTD and the S2 domain, whereas the RBD is largely glycan free (Watanabe, Allen et al. 2020, Zhao, Praissman et al. 2020). Consequently, it is unsurprising that the most antigenic domain on spike is the RBD, where the vast majority of neutralizing antibodies have been shown to bind. A comprehensive mapping of the epitopes from 1,640 neutralizing monoclonal antibodies (mAbs), all targeting the RBD, revealed 12 epitope groups (Cao, Yisimayi et al. 2022). This data, combined with previous studies mapping the epitopes of antibodies targeting spike, reveal a total of 19 mAb epitope groups, including 7 on the NTD (Wang, Muecksch et al. 2022). Very few anti-S2 antibodies have been shown to be effective therapeutic options (Wec, Wrapp et al. 2020), likely due to the shielding effect of S2 glycans (Grant, Montgomery et al. 2020).

The mechanism by which omicron variants of SARS-CoV-2 (e.g., BA.1, BA.4, BA.5 and XBB) escape the neutralizing abilities of antibodies generated against spike proteins from preceding variants, whether by vaccination or infection, is largely attributed to the extensive number of mutations accumulated in spike (Greaney, Loes et al. 2021, Starr, Greaney et al. 2022, Dadonaite, Crawford et al. 2023). Compared to wild-type SARS-CoV-2 spike, omicron BA.1 spike has 37 amino acid residue differences, with almost half located in the RBD domain (Mannar, Saville et al. 2022). The omicron BA.4/BA.5 variants, which have identical spike proteins (Tegally, Moir et al. 2022), have additional mutations (including the L452R substitution first seen in the delta variant), that render many previously broadly neutralizing antibodies ineffective (Cao, Yisimayi et al. 2022, Hachmann, Miller et al. 2022, Wang, Guo

et al. 2022). Of the monoclonal antibodies (mAbs) that previously received emergency use authorization (EUA) by the FDA for the treatment of SARS-CoV-2 infection, even cilgavimab and bebtelovimab that were respectively moderately and highly efficacious against omicron BA.5, are no longer effective against the current circulating variants XBB, BQ.1.1 and related sublineages (Takashita, Yamayoshi et al. 2022, Focosi, Quiroga et al. 2023, Imai, Ito et al. 2023). As a result, no mAb therapy is currently approved by the FDA for treatment of SARS-CoV-2 infection (www.fda.gov).

Nanobodies, single-domain antibodies derived from a unique heavy chain-only class of llama antibodies, present numerous therapeutic benefits compared to mAbs. Their smaller size and increased stability make them more resistant to denaturation, simpler to produce, and easier to modify in order to adjust properties such as immunogenicity and half-life (Muyldermans 2013). One potential advantage for neutralizing the spike protein is their compact size and distinctive binding attributes, which allow them to access and bind to epitopes that mAbs cannot reach. Consequently, while the antigenic evolution of the spike protein in response to antibodies has largely rendered mAbs ineffective in a therapeutic context, it remains uncertain how this applies to nanobodies. Moreover, the diminutive size of nanobodies enables them to bind concurrently to a single antigen through non-overlapping epitopes, making them well-suited for creating nanobody mixtures with the potential for highly synergistic effects (Fridy, Li et al. 2014, Mast, Fridy et al. 2021).

Here, we demonstrate that a subset of our previously published repertoire of nanobodies, generated against spike from the ancestral SARS-CoV-2 virus (Mast, Fridy et al. 2021), retains efficacy against circulating variants of concern (VoC), including omicron BA.4/BA.5. We show the power of nanobodies when working synergistically to create potent neutralizing mixtures against the different VoCs. We also predict that a subset of these nanobodies will remain efficacious against the circulating XBB and BQ.1.1 sublineages. Our study underscores the importance and versatility of large, diverse repertoires of nanobodies, in their potential to create long-term therapeutic options against rapidly evolving infectious agents such as the SARS-CoV-2 virus.

Results and Discussion

Nanobodies generated against wild-type SARS-CoV-2 remain efficacious against delta, omicron BA.1 and omicron BA.4/5, targeting all major regions of spike

From the original nanobody repertoire that we generated against SARS-CoV-2 wild-type spike protein (Mast, Fridy et al. 2021), representative nanobodies from all 10 structurally mapped epitope groups that we previously identified (Mast, Fridy et al. 2021, Cross, Fridy et al. 2023), were selected for SARS-CoV-2 pseudovirus (PSV) neutralization assays against the SARS-CoV-2 delta and omicron BA.1 strains (**Fig. 1**). Of the 41 nanobodies tested, 35 remained efficacious against at least one variant, where 28 neutralized delta, 23 neutralized omicron BA.1, and 15 neutralized both. The RBD groups I, I/II, II, I/IV and IV (where

nanobodies whose epitopes could not be distinguished between two groups are demarcated I/II and I/IV) and the anti-S2 groups (groups IX and X) contain a high number of nanobodies that neutralized delta.

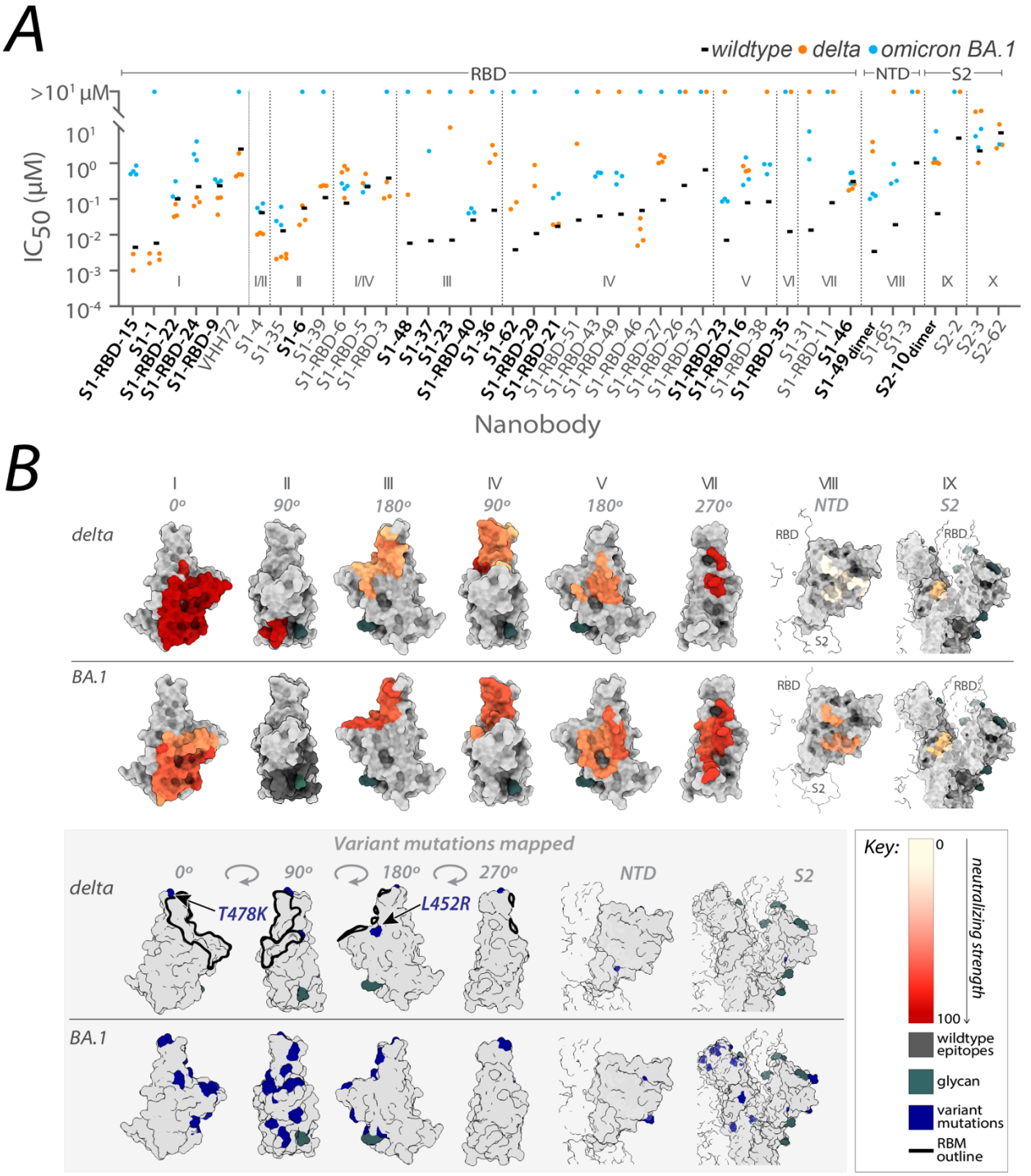

Figure 1. (See following for legend)

Figure 1. **Nanobody repertoires generated against wild-type SARS-CoV-2 remains efficacious.** Nanobodies targeting the S1-RBD, S1 non-RBD, and S2 portions of spike effectively neutralize lentivirus pseudotyped with delta and omicron BA.1 SARS-CoV-2 spikes (PSV) from infecting ACE2 expressing HEK293T cells. (A) The half-maximal inhibitory concentration (IC50) is reported for the indicated nanobodies against wild-type (Mast, Fridy et al. 2021), delta, and omicron BA.1 PSV. Nanobodies are grouped by epitope and arranged within each epitope by neutralization efficacy against the wild-type PSV. n ≥ 4 (B) The structure of the RBD of spike delta (PDB ID: 7SBO) and omicron BA.1 (PDB ID: 7T9K) is shown, with heat-mapped epitopes of neutralization colored from pale white (epitopes with weak neutralization against SARS-CoV-2) to dark red (strong neutralization against SARS-CoV-2). The color bar scale for each epitope is the neutralizing strength of each nanobody epitope, which is the normalized -log ratio of nanobody binding (IC50) of variant to wild-type SARS-CoV-2 Spike S1. A higher value of -log ratio corresponds to potent neutralization of the variant by the nanobody. All structure representations were created on ChimeraX (Pettersen, Goddard et al. 2021).

These observations are consistent with data from mAbs approved by the FDA, where nanobody epitopes from groups I, II and IV (**Fig. 1B**) overlap with the epitopes of five mAbs (grouped into three classes on RBD: class I, class II and class III) effective against delta: three class I (etesivimab, casirivimab and amubarvimab) (Greaney, Starr et al. 2021, Li, Xue et al. 2021, Planas, Veyer et al. 2021, Takashita, Yamayoshi et al. 2022, Cox, Peacock et al. 2023) and two class III (imdemivab and bebtelovimab) (Cox, Peacock et al. 2023). Additionally, the majority of our group I and II nanobodies neutralized delta better than wild-type (**Fig.1**), as observed with the mAb etesivimab (Wang, Li et al. 2022, Cox, Peacock et al. 2023). In comparison, groups I, I/II, I/IV, V, VII, VIII and the anti-S2 nanobodies contained the majority of omicron BA.1 neutralizers, though here the neutralization potency of many nanobodies was decreased compared to wild-type. This decrease in neutralization potency largely correlates with the accumulation of omicron BA.1 specific mutations throughout the RBD, which likely alters the epitope-binding site of these nanobodies, weakening their interaction with BA.1 spike (**Fig. 1B**). Concomitantly, groups I, I/II, I/IV and the anti-S2 nanobody groups contain nanobodies able to neutralize both delta and omicron BA.1. These results demonstrate the effectiveness of our original nanobody cohort against delta and omicron BA.1, targeting all major regions of spike.

Of the nanobodies that neutralized both delta and omicron BA.1, representatives from each of the nanobody epitope groups were selected for SPR analysis, where S1 binders with mapped epitopes that neutralized one or both variants well, were prioritized. The binding data as determined by SPR experiments performed against either spike S1 domain or RBD from delta and omicron BA.1, largely correlated with the neutralization data, where nanobodies that retained binding to the spike variant also neutralized the virus. We also tested this cohort for binding to omicron BA.4/BA.5 RBD using SPR, revealing that almost all the nanobodies in group I, I/II, II and I/IV retained binding to omicron BA.4/BA.5. Based on our previously mapped nanobody epitopes on spike (Mast, Fridy et al. 2021), these four groups appear to at least partially overlap with the spike epitope of the potent omicron BA.4/5 neutralizing mAb formerly FDA-approved, bebtelovimab (**Fig. S1**) (Focosi, Quiroga et al. 2023). The remaining six nanobody groups tested, including the major nanobody groups III and IV, showed no detectable binding to omicron BA.4/BA.5 RBD, save for RBD-40 (group III) and RBD-46 (group IV), which exhibited a ~40-fold and ~20-fold decrease in affinity respectively, compared to wild-type. The likely reason behind this loss of binding is

the concentration of omicron BA.4/BA.5 specific mutations that overlap with the epitope regions of the affected nanobodies, resulting in epitopes altered enough to abolish or significantly reduce binding (**Fig. 2B**). Interestingly, one nanobody, S1-46 (group VII, **Fig 1B and 2B**) retained wild-type binding affinity to RBDs from delta, omicron BA.1, and omicron BA.4/BA.5 (**Fig. 2, Table 1**). S1-46 binds a region on spike that is conserved across all variants to date and is not targeted by any of the mAbs that previously received EUA by the FDA (Cox, Peacock et al. 2023).

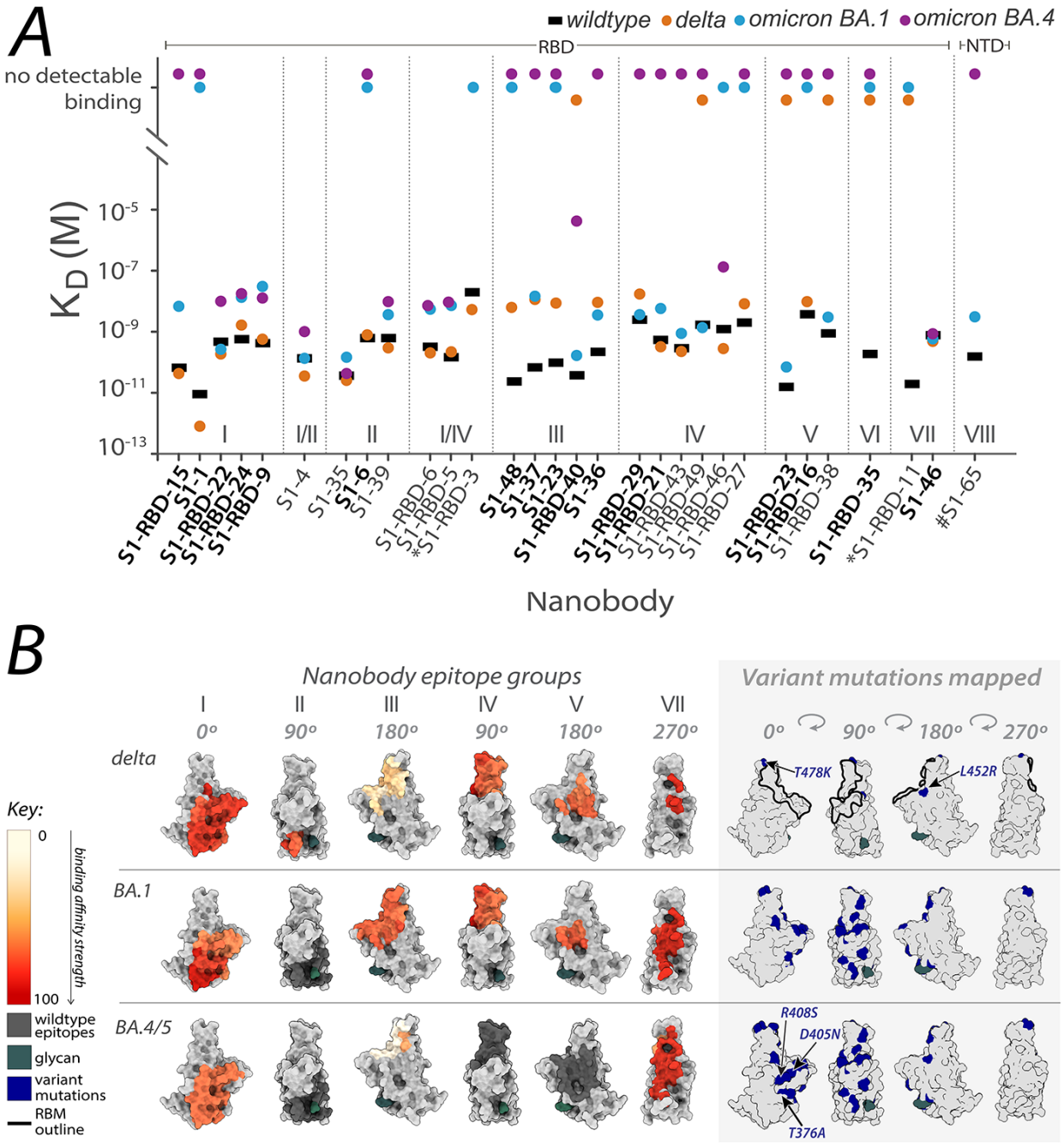

Figure 2. (See following for legend)

Figure 2. **Affinities of the nanobody repertoire against SARS-CoV-2 variants. (A)** Each nanobody is plotted against their affinity (K_D) for SARS-CoV-2 Spike S1 from wild-type, delta and omicron BA.1 and BA.4 strains. Nanobodies are characterized into their respective epitope groups according to Mast et al (Mast, Fridy et al. 2021). **(B)** The structure of the RBD of spike delta (PDB ID: 7SBO), omicron BA.1 (PDB ID: 7T9K) and omicron BA.4 RBD (modeled) is shown, with heat-mapped epitopes of binding colored from pale white (epitopes with weak binding against SARS-CoV-2) to dark red (strong binding against SARS-CoV-2). The nanobodies that contributed to epitope mapping are in bold in panel A. The color bar scale for each epitope shows the binding affinity strength of each nanobody epitope, which is the normalized -log ratio of nanobody binding (K_D) of variant to wild-type SARS-CoV-2 Spike S1. A higher value of -log ratio corresponds to strong binding of the nanobody to the variant. S1-RBD-16 showed binding to omicron BA.1 in ELISA. *S1-RBD-11 was not tested against omicron BA.4 and #S1-65 was not tested against BA.1. All structure representations were created on ChimeraX (Pettersen, Goddard et al. 2021).

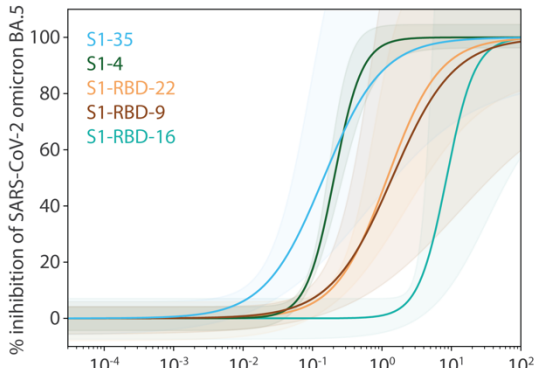

Guided by the SPR results against omicron BA.4/BA.5 RBD, nanobody neutralization of live BA.5 was performed using the plaque reduction neutralization test (PRNT) as previously described (Mast, Fridy et al. 2021). The results showed that all 5 nanobodies tested neutralized omicron BA.5 live virus (**Fig. 3**), supporting our SPR observations, to reveal our nanobody repertoire generated against wildtype spike has retained efficacy against omicron BA.4/BA.5.

Figure 3. **Potent neutralization by broadly active nanobodies.** Nanobodies targeting the S1-RBD of spike and raised against the original wild-type sequence remain highly efficacious in neutralizing an evolved variant of SARS-CoV-2, omicron variant BA.5. Neutralization curves are plotted from the results of a plaque-forming reduction neutralization test with the indicated nanobodies. Serial dilutions of each nanobody were incubated with ~200 SARS-CoV-2 virions for 60 min and then overlaid on a monolayer of TMPRSS2-expressing Vero E6 cells. After 72 h, cells were fixed and stained with crystal violet stain (1% w/vol in 20% ethanol) to visualize individual viral plaques. Plaques were enumerated for each nanobody dilution and used to fit the neutralization curves depicted in the figure. The colored shaded areas denote 90% confidence intervals for each fitted curve. $n \geq 3$.

Impact of spike structural differences across variants on nanobody binding and neutralization potency.

The numerous structural differences observed in the spike protein of the delta and omicron sublineages compared to wild-type, has enabled these variants to escape the neutralizing effect of most mAbs, with only one clinically approved mAb retaining potency against omicron BA.4/BA.5 (Takashita, Yamayoshi et al. , Cox, Peacock et al. , Focosi, Quiroga et al.). These structural differences have also somewhat affected our nanobody cohort, likely playing a role in the differential binding and neutralizing abilities observed against the three tested variants (delta, omicron BA.1 and omicron BA.4/5). Notably, all but one of our nanobodies in groups I, I/II and II, displayed *better* neutralizing ability against delta compared to wild-type (**Fig. 1**). It is possible that this difference is due to the delta spike trimer's preference for the up orientation of its RBDs, resulting from the increased dynamics in its S1 domain compared to wild-type (Wang, Liu et al. 2022); this more 'open' state likely allows greater accessibility to the epitopes of these nanobody groups, for net stronger binding. Additionally, the absence of delta-specific mutations within the epitope regions of

groups I and II preserves their integrity for nanobody binding (**Fig. 1B and 2B**). For the remaining RBD nanobody groups, we are likely observing the impact of the two delta mutations T478K and L452R on nanobody binding and neutralization. These two mutations lie within the mapped epitope regions of group III, IV and V nanobodies (**Fig. 1B and 2B**), which may alter the epitopes of many of these nanobodies enough to negatively impact both binding and neutralization. Importantly, the L452R mutation seems to be a key substitution that contributes to reduced or abolished neutralizing abilities of many mAbs (Laurini, Marson et al. 2021, Starr, Greaney et al. 2021, Starr, Greaney et al. 2021). Antibodies that rely on L452 to create hydrophobic interactions within their epitope will most likely have their binding greatly disrupted with a substituted arginine. Coupled with the stronger affinity between ACE2 and spike caused by L452R (Motozono, Toyoda et al. 2021, Yan, Hou et al. 2022), this substitution can greatly lessen the neutralization ability of nanobodies and antibodies targeting this region.

Unlike wild-type, the spike trimer of omicron BA.1 favors a one-RBD up confirmation (Zhao, Zhou et al. 2022). Though this conformation may facilitate access of our nanobodies to their epitopes on RBD, unlike delta, omicron BA.1 contains many unique mutations distributed throughout the RBD domain that overlap or flank the epitopes of almost all our nanobody groups (**Fig. 1B and 2B**). These mutations likely alter the epitopes of our nanobodies and may be the major contributing factor to the observed decrease in binding affinity and neutralizing potency of our nanobodies against omicron BA.1 (**Fig. 1A and 2A**). However, the following cohort of nanobodies retained binding and neutralizing ability similar to wild-type against omicron BA.1: S1-RBD-22, S1-RBD-9 (both Group I, Class I), S1-4 (Group I/II, Class III), S1-RBD-5 (Group I/IV, Class III), S1-46 (Group VII) and members of Group X. The additional mutations on the spike of omicron BA.4/BA.5, many of which overlap with our nanobody epitopes, are predicted to further impact the binding of our nanobody repertoire to this variant. For example, omicron BA.4/BA.5 re-introduces the key L452R substitution from delta, which when combined with the accumulated mutations on spike from omicron precursor sub-lineages, could be responsible for the observed loss of binding of numerous nanobodies in groups III, IV and V. Furthermore, the differential binding and neutralizing abilities of group I and group II nanobodies against omicron variants BA.4/5 may be because of the T376A, D405N and R408S substitutions, which lie within and near the epitope regions of groups I and II respectively (**Fig. 2B**). Importantly, at least 5 nanobodies from groups I, I/II, II and V retained neutralization activity against omicron BA.5 (**Fig. 3**), demonstrating the broad specificity of this set of nanobodies.

Nanobodies that lose neutralization ability can still bind spike

Our SPR experiments largely correlated with the neutralization data: nanobodies that showed binding to spike also neutralized the virus, and where the binding affinity decreased significantly, a loss of neutralization ability was observed. This was seen with the group III nanobodies S1-23 and S1-37 against both delta and omicron BA.1, where the significantly decreased binding affinity correlated to decreased neutralization potency, which is likely due

to the L452R mutation against delta, and the large number of amino acid substitutions compared to wild-type for omicron BA.1 (see above). However, we observed instances where nanobodies retained binding to spike yet no longer neutralized the virus. Nanobodies S1-36, S1-39 and S1-RBD-29 showed binding to omicron BA.1 (**Fig. 2A**), yet none neutralized the variant in the pseudovirus assay (**Fig. 1A**). These nanobodies are in groups III, II and IV respectively (**Fig. 2B**), epitope regions that contain numerous omicron BA. 1 mutations. For all three nanobodies, the mutations peppered throughout their epitope space have likely altered the binding landscape, resulting in decreased affinity (~100-fold for S1-36 and S1-39) and ineffective neutralization in vivo. Additionally, S1-RBD-29 binds an epitope that overlaps with the ACE2 binding site, and likely neutralizes the wild-type strain by blocking the ACE2 interaction (**Fig. 1B**). Alterations in the omicron BA.1 epitope may have changed the orientation of the nanobody as it binds, negating effective blocking of ACE2 binding and thus neutralization. In contrast, S1-37 bound both delta and omicron BA.1 with similar affinities (>100-fold decrease compared to wild-type), yet only neutralized omicron BA.1 (**Fig. 1A**). As mentioned above, the epitope of S1-37 overlaps with the delta L452R mutation (**Fig. 1B**), which has impacted the effectiveness of numerous neutralizing antibodies (Bian, Gao et al. 2021). It is possible that this mutation alone drastically weakens S1-37 binding to delta and consequently virus neutralization. Lastly, S1-RBD-43, whose epitope as a group IV binder is predicted to overlap with the ACE2 binding footprint (**Fig. 1B and 2B**), showed binding to delta with equal affinity to wild-type (**Fig. 2A**), yet does not neutralize delta (**Fig. 1A**). The delta mutation T478K is present within the epitope region of group IV (**Fig. 1B and 2B**), and was shown to significantly increase the interaction of delta spike for ACE2 by creating a new salt-bridge at the RBD / ACE2 interface (Cheng, Krieger et al. 2022). It may be that, as suggested for S1-RBD-29, the binding orientation of S1-RBD-43 has been altered allowing the RBD to maintain an interaction with ACE2 despite the presence of S1-RBD-43, thus rendering the nanobody ineffective in neutralizing delta.

Identification of variant-specific epitopes and broadly neutralizing epitope groups

The results of our neutralization assays and affinity measurements revealed that one-third of our original repertoire of 116 nanobodies (Mast, Fridy et al.) generated against wild-type SARS-CoV-2 remained effective binders/neutralizers of the variants tested, where nanobodies from 11 (including the 10 mapped epitopes) of the 18 nanobody groups are efficacious against the delta, omicron BA.1, and omicron BA.4/BA.5 lineages. The ability of nanobodies within a group to retain efficacy against different variants, coupled with the structural modeling data, allowed us to further refine our original six structurally modeled RBD epitope groups, for a total of 12 RBD epitope groups (**Fig. 4A**) compared to the three classes used to group mAbs (all RBD binders) previously approved for EUA by the FDA. When comparing our 12 RBD nanobody epitope groups to the three mAb classes, groups I, III, IV and VII overlap with class I binders; group II, III, IV and V overlap with class II binders; and group II, III and V overlap with class III binders (**Fig. S1**).

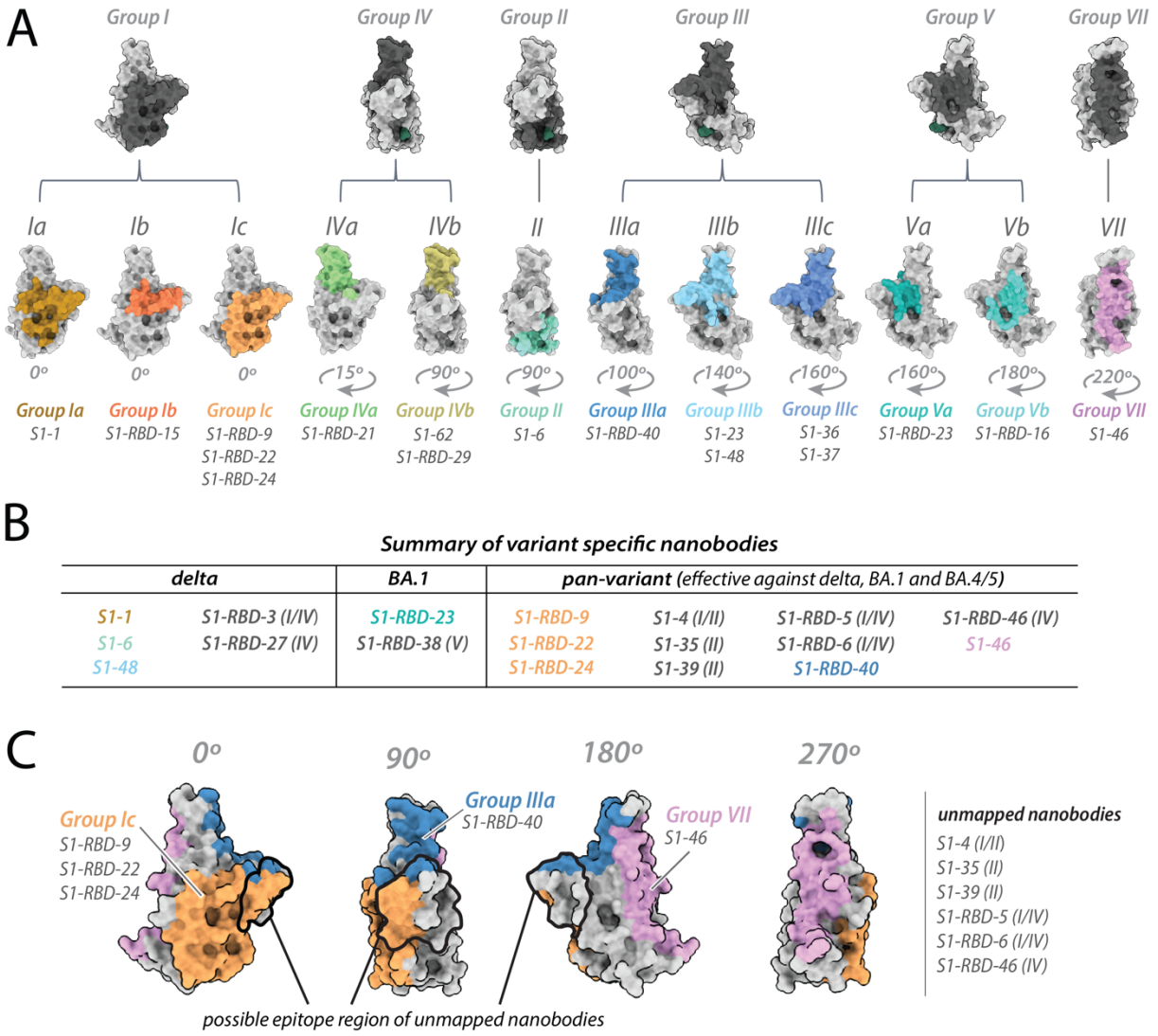

Figure 4. **Refining epitopes of the nanobody repertoire.** All epitopes are mapped on the structure of the RBD (PDB ID: 6M0J). **(A)** The epitopes of six RBD nanobody groups (colored dark gray) able to bind/neutralize one or more variants. Four of these epitope groups: I, III, IV and V were further refined resulting in an additional six epitope groups - creating a total of 12 epitope groups able to bind one or more variants of concern. **(B)** Summary of variant specific and pan-variant nanobodies. **(C)** Nanobody groups predicted to bind/neutralize the circulating variants XBB and BQ.1 and BQ.1.1. All structure representations were created on ChimeraX (Pettersen, Goddard et al. 2021).

Interestingly, the epitope footprint of many of our nanobody classes extends beyond those of the three mAb classes. For example, the majority of the epitope regions of the group I, II, V and VII nanobodies do not overlap with the mAb classes and are not a binding/neutralizing hotspot for mAbs (Almagro, Mellado-Sanchez et al. 2022, Cao, Yisimayi et al. 2022); instead, these epitopes extend away from the ACE2 binding site (**Fig 1.B and 2B**), as seen in particular with groups I, II and V nanobodies. These regions may be inaccessible to mAbs, possibly due to steric limitations, a property nanobodies readily overcome due to their small size. Additionally, our data allowed us to identify variant-

specific epitope groups (**Fig. 4B**) where: of the 26 nanobodies that showed binding/neutralization to delta, 6 were specific only for delta; of the 21 nanobodies that showed binding/neutralization to omicron BA.1, two were specific for omicron BA.1; none of the 10 nanobodies that retained binding to omicron BA.4 were specific only for omicron BA.4. Strikingly, we have in our cohort 11 nanobodies able to bind delta, omicron BA.1, and omicron BA.4/BA.5 (**Fig. 4B**), which we further predict will be effective binders against current circulating strains of the virus including omicron XBB and BQ1.1 (**Fig. 4C**).

Nanobody synergy involving a non-neutralizing nanobody

Previously, we showed that cocktails of nanobodies were more resistant to mutational escape (Mast, Fridy et al. 2021). Excitingly, not only was the barrier to mutational escape extremely enhanced, but for certain combinations of nanobodies, their mechanisms of neutralization were synergistic, providing far more potent neutralization in combination than predicted from the neutralization by either nanobody alone (Mast, Fridy et al. 2021). Our present observations of nanobodies that retained binding to variants of the spike RBD (**Table 1**) despite losing neutralization efficacy (**Fig. 1A; Table 1**) afforded us an opportunity to test whether the synergy observed for certain nanobody combinations was dependent on their ability to neutralize.

The synergistic S1-1 and S1-23 pair effectively neutralized the wild-type PSV with their epitopes on opposing surfaces of the RBD, permitting simultaneous binding and enhanced neutralization when delivered as a cocktail (Mast, Fridy et al. 2021) (**Fig. 1A, 2A, and 5A panel i**). While S1-1 remained efficacious against the delta variant of SARS-CoV-2, the L452R mutation in the delta RBD likely negatively impacted S1-23 (discussed above), weakening its binding affinity by ~1000-fold (12 nM) and negating its neutralization efficacy at concentrations <10 μM (**Fig. 1A, 2A, and 5A panel ii**). Surprisingly, when provided in combination with S1-1, which displays increased binding affinity and enhanced neutralization against the delta variant, S1-23 was able to further enhance the neutralization capabilities of S1-1, synergistically, at concentrations above 10^{-3} μM (**Fig. 5A panel ii**), by up to 42-fold. This synergistic interaction, however, did not apply to situations where extensive mutations are present in the RBD, such as in the omicron sublineages of SARS-CoV-2, which ablated the binding and neutralization efficacy of both S1-1 and S1-23 (**Fig. 1A, 2A, & 5A panel iii**).

We also tested the broadly neutralizing nanobody S1-RBD-22 in combination with S1-36 (**Fig. 5B**). Like S1-23, the epitope of S1-36 is opposite that of S1-RBD-22, permitting simultaneous binding to a single RBD (Mast, Fridy et al. 2021). However, while its neutralization efficacy dropped off when delivered to either delta or omicron BA.1 PSV alone, its ability to bind to its epitope was only marginally impacted (**Fig. 1A, 2A, 5B**). When provided in combination with S1-RBD-22, S1-36 synergistically enhanced by up to 80-fold the neutralization efficacy of S1-RBD-22 against both delta and omicron BA.1 PSB (**Fig. 5B panels ii, and iii**).

Table 1. Nanobody binding and neutralization characterization; related to Figure 2.

Group #	Nanobody	wildtype[#]				Delta				Omicron BA.1				Omicron BA.4/5			
		K_{on} ($M^{-1}s^{-1}$)	K_{off} (s^{-1})	K_D (M)	PSV IC_{50} (s.e.m) (nM)	K_{on} ($M^{-1}s^{-1}$)	K_{off} (s^{-1})	K_D (M)	PSV IC_{50} (s.e.m) (nM)	K_{on} ($M^{-1}s^{-1}$)	K_{off} (s^{-1})	K_D (M)	PSV IC_{50} (s.e.m) (nM)	K_{on} ($M^{-1}s^{-1}$)	K_{off} (s^{-1})	K_D (M)	IC_{50} (nM)
1	**S1-1**	6.50E+05	5.98E-07	9.20E-12	6.7(1.0)	1.27E+06	1.00E-06	7.87E-13	2.3(0.5)	No binding			NA	No binding			
	S1-RBD-9	2.85E+05	1.23E-04	4.30E-10	235(97.5)	(1)3.93E+05 (2)1.76E-03	(1)1.00E-03 (2)5.04E-04	5.69E-10*	85.2 (24.3)	6.05E+03	1.82E-04	3.01E-08	323 (20.8)	4.36E+05	5.49E-03	1.26E-08	966 (220)
	S1-RBD-15	7.52E+06	4.95E-04	6.58E-11	4.6(1.2)	2.55E+06	1.08E-04	4.25E-11	2(0.9)	1.95E+06	1.32E-02	6.79E-09	617(87)	No binding			
	S1-RBD-22	9.24E+05	4.42E-04	4.78E-10	100(0.1)	(1)1.07E+06 (2)9.10E-04	(1)6.25E-04 (2)4.15E-04	1.83E-10*	46.4(12)	7.30E+05	1.91E-04	2.62E-10	179(68)	1.07E+06	1.05E-02	9.8E-09	976 (285)
	S1-RBD-24	2.12E+06	1.22E-03	5.75E-10	221(4)	(1)5.74E+05 (2)1.61E-03	(1)2.62E-03 (2)9.00E-04	1.64E-09*	85.5 (13.5)	(1)2.66E+05 (2)2.63E-03	(1)1.49E-02 (2)8.24E-04	1.34E-08*	2382 (878)	9.25E+05	1.62E-02	1.75E-08	
2	**S1-6**	5.92E+05	3.69E-04	6.22E-10	56.1(20.7)	3.19E+05	2.48E-04	7.77E-10	37.3 (14.7)	No binding				No binding			
	S1-35	2.70E+06	9.77E-05	3.62E-11	12.5(0.1)	5.83E+05	1.48E-05	2.54E-11	28(5.2)	5.20E+05	7.56E-05	1.45E-10	49(13.6)	1.02E+06	4.35E-05	4.27E-11	182(55)
	S1-39	1.68E+06	1.06E-03	6.30E-10	111(4.0)	2.30E+06	6.73E-04	2.92E-10	236(3.8)	(1)1.14E+05 (2)5.04E-03	(1)5.48E-03 (2)4.12E-04	3.62E-09*		7.59E+04	7.3E-04	9.61E-09	
3	**S1-23**	1.09E+06	1.07E-04	9.78E-11	5.7(2.2)	2.33e+5	2.85e-3	1.23E-08	NA	No binding				No binding			
	S1-36	7.87E+06	1.72E-03	2.18E-10	48.5(21.1)	(1)7.90E+05 (2)2.11E-03	(1)2.28E-02 (2)9.57E-04	9.00E-09*	1387 (209)	(1)1.19E+06 (2)2.02E-03	(1)1.64E-02 (2)6.80E-04	3.47E-09*	NA	No binding			
	S1-RBD-40	7.47E+05	2.77E-05	3.71E-11	25.6(5.9)	No binding			NA	2.25E+05	3.71E-05	1.65E-10	46.1 (4.7)	(1)2.54E+04 (2)6.23E-03	(1)3.07E-01 (2)3.29E-03	4.17E-06*	NA<10uM)
	S1-37	4.03E+06	2.75E-04	6.82E-11	6.8(0.7)	1.18E+05	1.35E-03	1.14E-08	NA	1.38E+06	1.99E-02	1.44E-08	NA	No binding			
	S1-48	2.61E+06	6.22E-05	2.39E-11	5.82(0.5)	5.74E+05	3.54E-03	6.18E-09		No binding				No binding			
4	**S1-RBD-21**	3.15E+06	1.71E-03	5.45E-10	17.3(3.1)	(1)1.82E+06 (2)8.40E-04	(1)1.98E-03 (2)3.48E-04	3.18E-10*	21(1.3)	(1)1.90E+05 (2)2.17E-03	(1)3.16E-03 (2)1.16E-03	5.80E-09*	113(14)	No binding			
	S1-RBD-27	6.19E+06	1.24E-02	2.00E-09	163(71.4)	(1)4.06E+05 (2)5.17E-03	(1)1.48E-02 (2)1.51E-03	8.24E-09*	1390 (198)	No binding			NA	No binding			
	S1-RBD-29	5.36E+05	1.35E-03	2.51E-09	9.53(1.0)	(1)1.80E+05 (2)9.46E-04	(1)6.99E-03 (2)7.32E-04	1.69E-08*	564(332)	3.30E+04	1.20E-04	3.63E-09	NA	No binding			
	S1-RBD-43	6.21E+05	1.82E-04	2.92E-10	33.6(1.3)	5.39E+06	1.19E-03	2.21E-10	NA	4.79E+05	4.23E-04	8.83E-10	1032(543)	No binding			
	S1-RBD-46	4.69E+05	5.79E-04	1.23E-09	48.0	1.11E+06	3.12E-04	2.81E-10	8.7(3)	No binding			NA	(1)2.17E+05 (2)1.60E-02	(1)1.38E-01 (2)4.15E-03	1.31E-07*	1020
	S1-RBD-49	3.15E+05	5.34E-04	1.69E-09	37.6(5.6)	No binding				2.54E+05	3.48E-04	1.37E-09	404 (145)	No binding			
5	**S1-RBD-16**	1.68E+04	6.25E-05	3.73E-09	79.2(4.2)	3.13E+04	3.04E-04	9.74E-09	688 (72.6)	No binding				No binding			
	S1-RBD-23	2.89E+06	4.61E-05	1.59E-11	7.31(0.4)	No binding			NA	7.91E+05	5.43E-05	6.87E-11	91.7 (5.2)	No binding			
	S1-RBD-38	1.12E+06	9.84E-04	8.79E-10	84.6(22.7)	No binding			NA	2.37E+05	7.06E-04	2.98E-09	790 (146)	No binding			NA<10uM
6	**S1-RBD-35**	1.33E+06	2.50E-04	1.88E-10	12.3(2.4)	No binding				No binding				No binding			
7	**S1-46**	2.22E+05	1.70E-04	7.66E-10	312(14.0)	6.93E+04	4.05E-05	5.85E-10	210.2 (26)	2.12E+05	1.24E-04	5.85E-10	412 (116)	1.27E+05	1.07E-04	8.46E-10	NA<10uM
8	**S1-65**	1.06E+06	1.67E-04	1.57E-10	7.3(6.0)	Not tested			NA	3.42E+05	1.05E-03	3.07E-09	517 (218)	No binding			
1/2	**S1-4**	1.26E+06	1.26E-04	1.37E-10	41.5(3.7)	1.38E+06	4.83E-05	3.51E-11	10.7(0.4)	6.00E+05	7.98E-05	1.33E-10	58.6 (9.2)	1.32E+06	1.32E-03	1.00E-09	148.6 (37.6)
1/4	**S1-RBD-3**	5.12E+05	1.01E-02	1.98E-08	384(18.7)	(1)3.27E+05 (2)1.62E-03	(1)5.54E-03 (2)7.42E-04	5.32E-09*	83.9	No binding				Not tested			
	S1-RBD-5	7.21E+06	1.05E-03	1.45E-10	174(3.3)	1.49E+06	3.29E-04	2.2E-10	280	(1)1.18E+05 (2)2.95E-03	(1)4.32E-03 (2)7.96E-04	7.75E-09*	204 (24.6)	1.19E+06	9.71E-03	8.19E-09	
	S1-RBD-6	3.48E+06	1.13E-03	3.24E-10	77.2(21.8)	(1)6.68E+05 (2)1.08E-03	(1)5.04E-04 (2)3.85E-04	1.99E-10*	542.3 (155.8)	(1)1.43E+05 (2)3.37E-03	(1)3.44E-03 (2)9.96E-04	5.49E-9*	233.8 (23)	8.72E+05	5.71E-03	6.55E-09	

[#]Values taken from (Mast, Fridy et al. 2021)

*Fit to a two-state mode

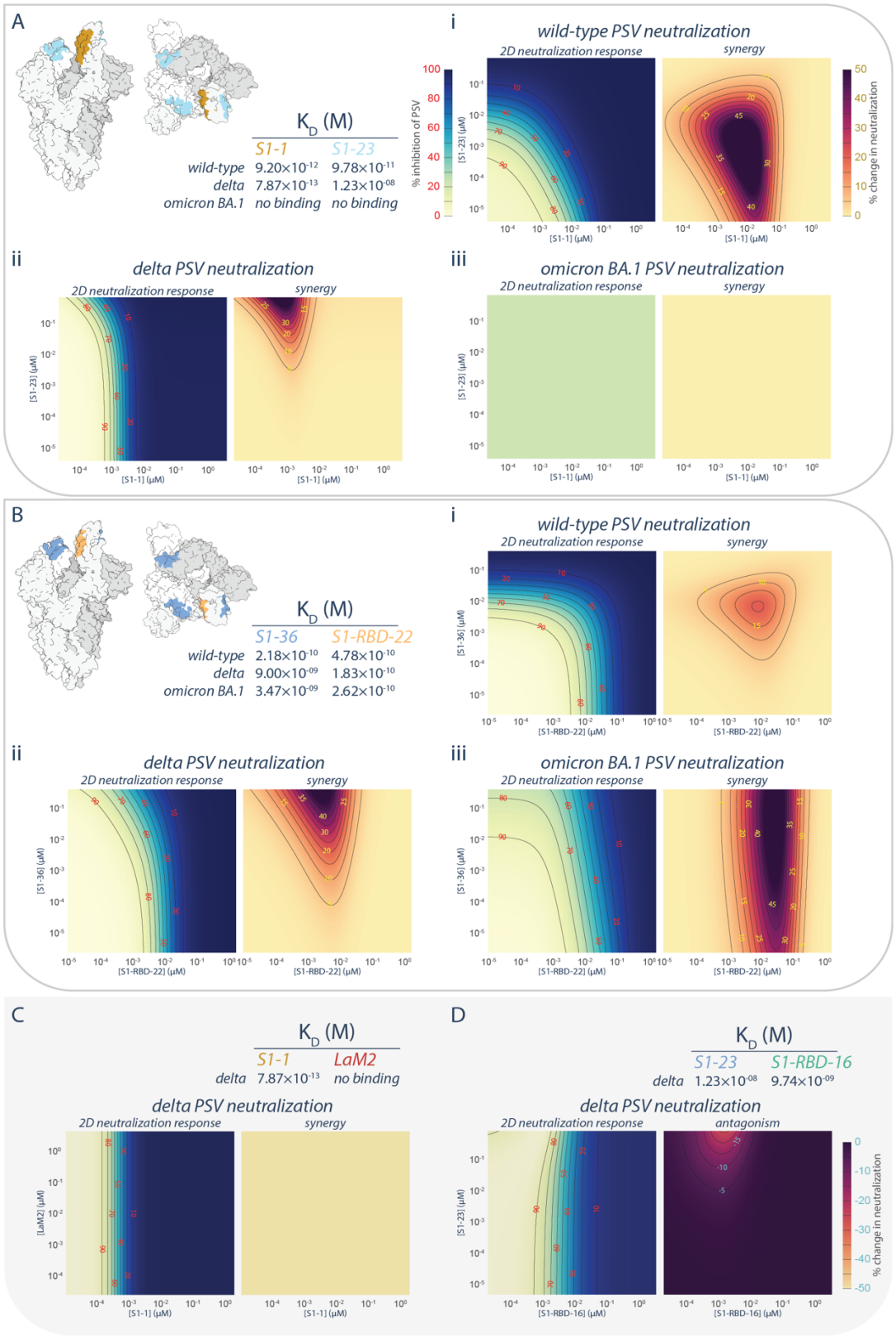

Figure 5. (See following for legend)

Figure 5. **Persistence of synergistic neutralization with nanobody cocktails against SARS-CoV-2 Variants of Concern.** (A) S1-1 synergizes with S1-23 in neutralizing SARS-CoV-2 pseudovirus. The upper left panel shows two representations of spike with the accessible S1-1 (dark goldenrod) and S1-23 (sky blue) epitopes (PDB ID: 6VYB). The measured affinities for S1-1 and S1-23 (Table 1) for the RBD of wild-type, delta, and omicron BA.1 are displayed. Both S1-1 and S1-23 neutralize wild-type (i), whereas only S1-1 neutralizes delta at the concentrations shown (ii). In spite of a lack of neutralization at these concentrations, S1-23, synergizes with S1-1 and enhances its neutralization of delta SARS-CoV-2 pseudovirus (ii). As neither S1-1 or S1-23 are able to bind to the RBD of omicron BA.1, neither nanobody neutralizes omicron BA.1 SARS-CoV-2 pseudovirus (iii). (B) S1-36 synergizes with S1-RBD-22 in neutralizing SARS-CoV-2 pseudovirus. As in A, the upper left panel shows two representations of spike with the accessible S1-36 (cornflower blue) and S1-RBD-22 (sandy brown) epitopes. The measured affinities for S1-36 and S1-RBD-22 are displayed. Both S1-36 and S1-RBD-22 neutralize wild-type (i), whereas only S1-RBD-22 effectively neutralizes delta and omicron BA.1 SARS-CoV-2 pseudovirus at the concentrations shown (ii and iii, respectively). However, S1-36 synergizes with S1-RBD-22 and enhances its neutralization of the three depicted SARS-CoV-2 pseudoviruses (i, ii, and iii). (C) An example of no interactions (synergistic or antagonistic) between S1-1 and LaM2 (Fridy, Li et al. 2014), a non-specific nanobody that does not bind the RBD of delta. (D) An example of antagonism, where higher concentrations of S1-23 interferes with the ability of S1-RBD-16 to neutralize delta SARS-CoV-2 pseudovirus. These nanobodies have adjacent epitopes on the RBD of spike and were previously shown to interfere with each other's binding to their respective epitope (Mast, Fridy et al. 2021). n = 4. Source data in Supplementary Table 1.

The synergies observed between S1-1 and S1-23, and between S1-RBD-22 and S1-36, are likely not due to pleiotropic effects, as providing the nonspecific LaM2 nanobody in combination with S1-1 had no impact on the neutralization efficacy of S1-1 against delta PSV (**Fig. 5C**). Furthermore, in the case of S1-23, binding to its non-neutralizing epitope on the RBD of delta PSV was able to induce dose-dependent antagonistic effects on the neutralizing efficacy of S1-RBD-16, which binds to a neighboring epitope that can be competitively blocked by S1-23 (**Fig. 5D**) (Mast, Fridy et al. 2021).

Conclusions

Collectively, our binding and neutralization data allowed us to identify the regions of spike in multiple VoC that remained vulnerable to our original repertoire of nanobodies raised against wild-type SARS-CoV-2 spike (**Fig. 6**) (Mast, Fridy et al. 2021). Unlike the epitope groups defining mAb binding sites on spike, many of our nanobody epitope groups remained efficacious in the neutralization of different VoC (**Fig 5 and 6**), possibly due to each nanobody's smaller epitope footprint allowing their access to regions of spike inaccessible to mAbs. However, the substantial changes on the surface of spike that has occurred as SARS-CoV-2 has evolved from one variant to the next has also negatively impacted many nanobodies by abolishing or weakening their binding and/or neutralization activity. This weakening is most evident for nanobodies directed against the NTD, and against the receptor binding motif that engages ACE2 (**Fig. 1B and 2B**).

Intriguingly, we discovered nanobodies that maintained binding capabilities while losing their neutralizing properties. This finding paves the way for engineering these nanobodies

through approaches like oligomerization, which has proven effective in boosting neutralization (Wrapp, De Vlieger et al. 2020, Mast, Fridy et al. 2021). Remarkably, we also showed that such non-neutralizing binders can nevertheless retain effectiveness as components of synergistic nanobody cocktails, suggesting their potential for widespread antiviral applications. This finding indicates that the mechanism of synergy can operate through epistatic interactions from binding alone, not solely through direct neutralization. Furthermore, these synergistic pairings hold promise as therapeutic options when formulated as multivalent hetero-oligomers.

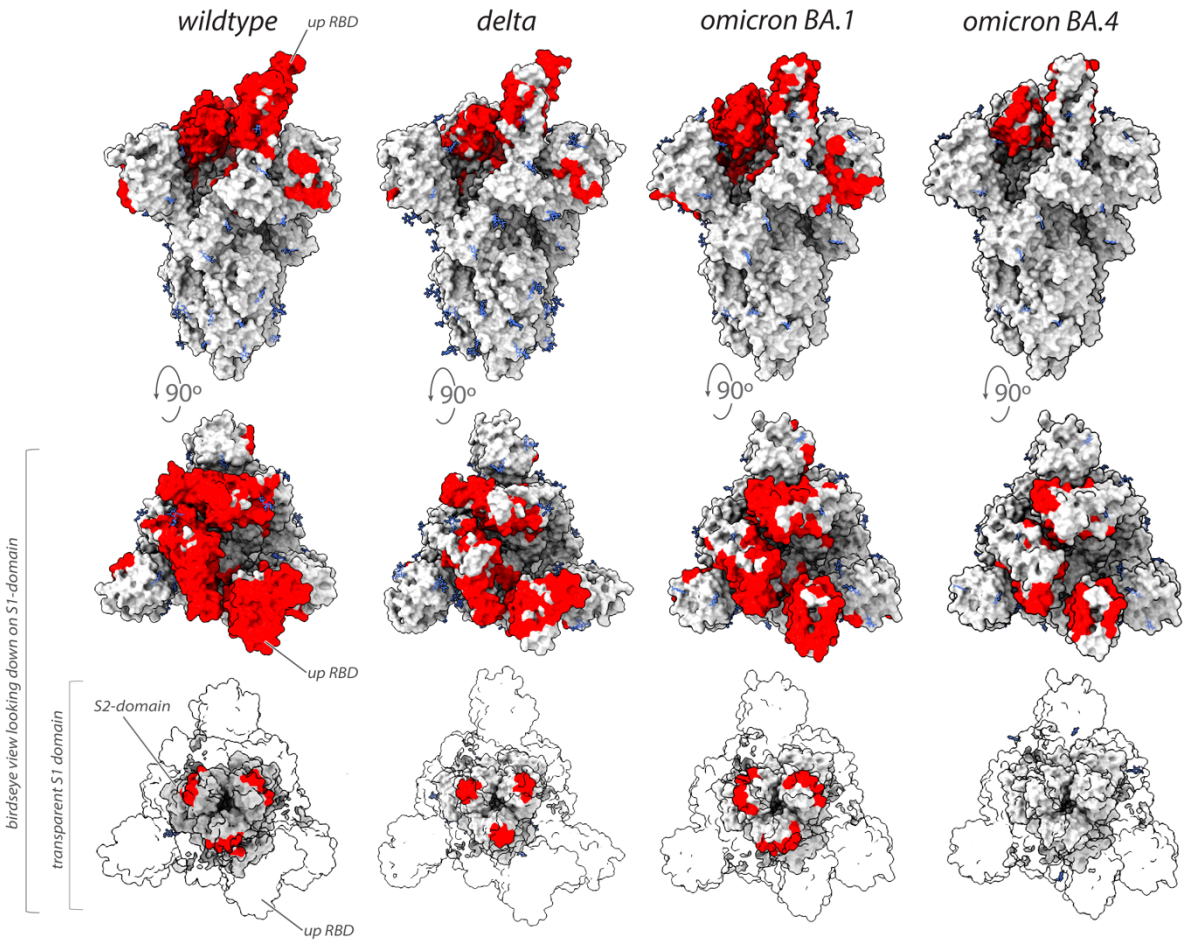

Figure 6. Nanobodies effective against circulation variants of concern. The nanobody epitopes (red) that retain effectiveness against wild-type (PDB ID: 7KNB), delta (PDB ID: 7V7O), omicron BA.1 and omicron BA.4 (the nanobody epitopes were mapped on PBD ID: 7XO5 for both BA.1 and BA.4 due to lack of suitable BA.4 structure). The spike trimer (*silver* where glycans are represented as *light blue* sticks) for each variant is displayed in three views: top = side-view of spike trimer; middle = birds-eye view looking down on the S1 domain and; bottom = birds-eye view (same as middle view) with the S1 domain made transparent to see the S2-domain. All structure representations were created on ChimeraX (Pettersen, Goddard et al. 2021).

In this study, we identified nanobodies that specifically recognize only certain SARS-CoV-2 variants (**Fig. 4B**), allowing for the possibility of distinguishing between different VoC. By utilizing these nanobodies as molecular probes in diagnostic tests, a unique "molecular fingerprint" could define each variant based on the combinations of nanobodies that bind to and recognize the specific virus particle. Consequently, this approach could enable the accurate and rapid diagnosis of SARS-CoV-2 infections as well as provide real-time identification of the specific variant causing the infection, thus enhancing surveillance and tailoring treatment strategies accordingly to optimize patient outcomes and control the spread of the virus.

Together, our findings highlight the strength and variety of the heavy chain-only category of llama antibody immune responses and, as a result, the extensive repertoires of high-affinity nanobodies. This result emphasizes the distinct benefits of nanobody technology, which enables extensive coverage of antigenic regions while simultaneously targeting multiple unique epitope sites. This approach paves the way for investigating a wide range of therapeutic options against rapidly-evolving proteins like the SARS-CoV-2 spike protein, ultimately aiding in our preparedness and defense against future pandemics or major outbreaks.

Materials and Methods

K_D measurements.

Series S CM5 sensor chips (Cytiva) were immobilized with recombinant delta Spike S1, delta RBD and omicron RBD at 12.5 ug/mL, 10 ug/mL and 15 ug/mL respectively using EDC/NHS coupling chemistry according to the manufacturer's instructions. K_D measurements were performed on a Biacore 8k (Cytiva) as previously described (Mast, Fridy et al. 2021), using 5-8 concentrations of each nanobody. Data was processed and analyzed using the Biacore Insight Evaluation software.

Structural modeling

Integrative structure modeling of nanobody epitopes on the different variant spike proteins, proceeded through the standard four-stage protocol (Kim, Fernandez-Martinez et al. 2018, Webb, Viswanath et al. 2018, Rout and Sali 2019, Sali 2021, Saltzberg, Viswanath et al. 2021). This protocol was implemented using the *Python Modeling Interface* package, a library for modeling macromolecular complexes based on the open-source *Integrative Modeling Platform* software, version 2.15.0 (https://integrativemodeling.org). Only (a subset of) nanobodies with pre-determined experimental escape mutations on the Wuhan spike structure were selected for modeling. Separate models were computed for rigid-receptor-rigid ligand-type binary docking of representative nanobodies from Group-1 (S1-1, S1-RBD-[9, 15, 22, 24]), Group-2 (S1-6), Group-3 (S1-[23, 36]), Group-4 (S1-RBD-[21, 29]), Group-5 (S1-RBD-[16, 23]), Group-7 (S1-46), Group-8 (S1-49) and Group-9 (S2-10), to the variant spike structures. S1-49 was docked to a monomeric S1-NTD domain, S2-10 was docked to

the trimeric S2 (ecto-) domain, while the remaining nanobodies were docked to the S1-RBD domain. Monomeric S1-RBD spanning amino acid residues 333-526 was represented using the 2.45 Å crystal structure of the ACE2 bound RBD (6M0J.E; (Lan, Ge et al. 2020)) for the original virus, the 4.30 Å cryo-EM structure of up-RBD pre-fusion spike (7SBO.A; (Zhang, Xiao et al. 2021)) for the delta variant, the ACE2 bound 2.45 Å cryo-EM spike structure (7T9K.B; (Mannar, Saville et al. 2022)) for the omicron BA.1 variant and a structure predicted using AlphaFold-2 for the omicron BA.4/BA.5 variant. For the original virus, monomeric S1-NTD, spanning amino acid residues 16-305, was represented using the crystal structure of the S2M28 Fab bound NTD (7LY3.A; (McCallum, De Marco et al. 2021)), while trimeric S2 was represented using the amino residues 689-1162 (for each monomer) from the 2.9 Å cryo-EM structure 6XR8 (Cai, Zhang et al. 2020). NTD and S2 structures for delta and omicron variants were extracted from the corresponding whole spike structures.

Structural models for all 15 nanobodies and the omicron BA.4 RBD were built with the ColabFold implementation of AlphaFold2 (Jumper, Evans et al. 2021, Mirdita, Schutze et al. 2022). The protocol included automatic refinement of the CDR loops through an all-atom energy minimization of the AlphaFold2-predicted structure using the AMBER molecular mechanics force field (Hornak, Abel et al. 2006). We verified that the predicted nanobody structures are within 3-4 Å backbone RMSD from the comparative models of these nanobody sequences published previously (Mast, Fridy et al. 2021). The CDR region boundaries in the nanobody structures were assigned using the FREAD algorithm as implemented within the SabPred web server (Rausch 1991).

To make structural sampling sufficiently efficient, the system was represented at a resolution of one bead per residue, and the receptors and all nanobodies were treated as rigid bodies. For each nanobody, alternate binding modes were scored using spatial restraints enforcing receptor-ligand shape complementarity, cross-link satisfaction and proximity of CDR3 loops on the nanobodies to escape mutant residues on the corresponding receptor. With the receptor fixed in space, 1,200,000 alternative docked nanobody models were produced through 20 independent runs of replica exchange Gibbs sampling based on the Metropolis Monte Carlo algorithm, where each Monte Carlo step consisted of a series of random rotations and translations of rigid nanobodies. The initial set of models was filtered to obtain a random subsample of 30,000 models, which were clustered by the structural similarity of their interfaces to the receptor; this similarity was quantified by the fraction of common contacts (fcc) between receptor and nanobody was used to characterize interface similarity between alternate nanobody poses (Rodrigues, Trellet et al. 2012). Binding poses from the most populated cluster were selected for further analysis. Five independent random subsamples of 30,000 models each were generated from the set of all models post-structural sampling, and the entire protocol of interface similarity-based clustering and top cluster selection was repeated each time. No significant differences among these five subsamples were observed in the satisfaction of restraints. Structural differences among the variants, as well as between AlphaFold2 models and

previously published comparative models of nanobodies, lead to differences in binding modes of the same nanobody to different spike variants. Thus, for the sake of consistency we limit our comparison to the receptor epitopes, which are defined as all receptor atoms that are within 6 Å of the framework and CDR regions of the nanobodies (excluding the flexible N- and C-terminal regions). Although we don't include the nanobody paratopes in our analysis, we verified that all binding modes are primarily through CDR3, except for the CDR1 contribution to the binding of S1-1 and S1-RBD-15 to the RBD, for all variants. Relative differences in binding affinity (Kd) and neutralization potential (IC50) between the original virus and other variants (delta and omicron) were projected onto the Wuhan epitopes to create the heatmaps in Figures 1B and 2B. Relative differences were reported as $-log(\frac{Kd^{variant}}{Kd^{wuhan}})$ or $-log(\frac{IC50^{variant}}{IC50^{wuhan}})$ and normalized to the range from 0-100.

Integrative models of nanobody epitopes on the spike protein were computed on the Wynton HPC cluster at UCSF. Receptor epitopes were visualized in UCSF ChimeraX (Pettersen, Goddard et al. 2021). Files containing input data, scripts and output results are available at https://github.com/integrativemodeling/nbspike/tree/main/integrative_modeling_VOC. Structure predictions using ColabFold utilized the "AlphaFold2_batch" notebook, with the default settings. All modeled structures were subjected to molecular-mechanics-based relaxation, followed by using the model with the top pLDDT score was selected for the integrative modeling pipeline.

Cell lines

TMPRSS2-expressing Vero E6 cells, 293T/17 cells and 293T-hACE2 cells were cultured as described previously (Mast, Fridy et al. 2021). Briefly, TMPRSS2+ Vero E6 cells were cultured at 37°C in the presence of 5% CO2 in medium composed of in high-glucose Dulbecco's modified Eagle's medium (DMEM, Gibco) supplemented with 10% (v/v) FBS and 1 mg/ml geneticin. 293T/17 were cultured at 37°C in the presence of 5% CO2 in a medium composed of DMEM supplemented with 10% (v/v) FBS and penicillin/streptomycin. 293t-hACE2 cells were cultured at 37°C in the presence of 5% CO2 in medium composed of DMEM supplemented with 10% (v/v) FBS, penicillin/streptomycin, 10 mM HEPES, and with 0.1 mM MEM non-essential amino acids (Thermo Fisher). All experiments were performed with cells passaged less than 15 times. The identities of cell lines were confirmed by chromosomal marker analysis and tested negative for mycoplasma using a MycoStrip (InvivoGen).

Production of SARS-CoV-2 variant pseudotyped lentiviral reporter particles.

Pseudovirus stocks were prepared and titered as described previously (Mast, Fridy et al. 2021). Variant spike containing plasmids were combined with pHAGE-CMV-Luc2-IRES-ZsGreen-W (BEI Cat # NR-52516) (Crawford, Eguia et al. 2020), and psPAX using lipofectamine 3000 and cotransfected into 293T/17 cells. Pseudovirus was titered by

threefold serial dilution on 293T-hACE2 cells, as described previously (Mast, Fridy et al. 2021).

SARS-CoV-2 pseudovirus neutralization assay

Nanobodies were tested for their neutralization properties as described previously (Mast, Fridy et al. 2021). Briefly, threefold serial dilutions of nanobodies were incubated with pseudotyped SARS-CoV-2 for 1 h at 37°C. The nanobody-pseudovirus mixtures were then added in quadruplicate to 293T-hACE2 cells along with 2 µg/ml polybrene (Sigma). Cells were incubated at 37°C with 5% CO2. Infected cells were processed between 52 and 60 hr as described above. Infected cells were processed between 52 and 60 hr by adding equal volume of Steady-Glo (Promega), and firefly luciferase signal was measured using the Biotek Model N4 with integration at 0.5 ms. Data were processed using Prism 7 (GraphPad), using four-parameter nonlinear regression (least-squares regression method without weighting). All nanobodies were tested at least two times and with more than one pseudovirus preparation.

Nanobody synergy

Synergy experiments were performed as described previously, (Mast, Fridy et al. 2021). Briefly, a robotic liquid handler was used to prepare 2D matrices of threefold serial dilutions of two nanobodies and then mix these combinations with different variant pseudotyped SARS-CoV-2 for one h. After incubation with the virus, the mixture was overlaid on a monolayer of 293-hACE2 cells and left to incubate for 56 h. Luminescence was quantified as described above. Data were processed using the Bivariate Response to Additive Interacting Doses (BRAID) model (Twarog, Stewart et al. 2016) as implemented in the synergy software package for python (Wooten and Albert 2021).

SARS-CoV-2 stocks and titers

All experimental work involving live SARS-CoV-2 was performed at Seattle Children's Research Institute (SCRI) in compliance with SCRI guidelines for BioSafety Level 3 (BSL-3) containment. SARS-CoV-2 isolate CGIDR_SARS2 omicron BA.5 was obtained from an infected individual. An initial inoculum was diluted in Opti-MEM (Gibco) at 1:1000, overlaid on a monolayer of Vero E6 and incubated for 90 min. Following the incubation, the supernatant was removed and replaced with 2% (v/v) FBS in Opti-MEM medium. The cultures were inspected for cytopathic effects, and infectious supernatants were collected, cleared of cellular debris by centrifugation, and stored at –80°C until use. Whole viral genome sequencing and variant analysis was performed by the University of Washington Department of Laboratory Medicine & Pathology. Viral titers were determined by plaque assay using a liquid overlay and fixation-staining method, as described previously (Mendoza, Manguiat et al. 2020, Mast, Fridy et al. 2021).

ACKNOWLEDGEMENTS

We are very grateful to The Fisher Drug Discovery Resource Center (DDRC), Rockefeller University, and the rest of the Aitchison, Chait and Rout laboratories for intellectual support.

Funding:
G. Harold and Leila Y. Mathers Charitable Foundation (JDA, BTC, MPR)
Robertson Therapeutic Development Fund (JDA, BTC, MPR)
Jain Foundation (JDA, BTC, MPR)
National Institutes of Health grant P41GM109824 (JDA, BTC, AS, MPR)
National Institutes of Health grant R01GM083960 (AS)

Author contributions:
Conceptualization: JDA, BTC, MPR, NEK, PCF, FDM, JPO, TS
Methodology: JDA, BTC, MPR, NEK, FDM, JPO, TS, PCF
Investigation: NEK, FDM, JPO, TS, PCF
Visualization: JDA, BTC, MPR, NEK, PCF, FDM, JPO, TS
Funding acquisition: JDA, BTC, MPR, AS
Project administration: JDA, BTC, MPR
Supervision: JDA, BTC, MPR, AS
Writing – original draft: NEK, FDM, PCF, JPO, TS
Writing – review & editing: JDA, BTC, MPR, NEK, PCF, FDM, JPO, TS, AS

COMPETING INTERESTS

JDA, BTC, MPR, PCF, NEK, FDM, and JPO are inventors on a provisional patent describing the anti-spike nanobodies described in this manuscript.

REFERENCES

Almagro, J. C., G. Mellado-Sanchez, M. Pedraza-Escalona and S. M. Perez-Tapia (2022). "Evolution of Anti-SARS-CoV-2 Therapeutic Antibodies." Int J Mol Sci **23**(17).

Bian, L., Q. Gao, F. Gao, Q. Wang, Q. He, X. Wu, Q. Mao, M. Xu and Z. Liang (2021). "Impact of the Delta variant on vaccine efficacy and response strategies." Expert Rev Vaccines **20**(10): 1201-1209.

Cai, Y., J. Zhang, T. Xiao, H. Peng, S. M. Sterling, R. M. Walsh, Jr., S. Rawson, S. Rits-Volloch and B. Chen (2020). "Distinct conformational states of SARS-CoV-2 spike protein." Science **369**(6511): 1586-1592.

Cao, Y., A. Yisimayi, F. Jian, W. Song, T. Xiao, L. Wang, S. Du, J. Wang, Q. Li, X. Chen, Y. Yu, P. Wang, Z. Zhang, P. Liu, R. An, X. Hao, Y. Wang, J. Wang, R. Feng, H. Sun, L. Zhao, W. Zhang, D. Zhao, J. Zheng, L. Yu, C. Li, N. Zhang, R. Wang, X. Niu, S. Yang, X. Song, Y. Chai, Y. Hu, Y. Shi, L. Zheng, Z. Li, Q. Gu, F. Shao, W. Huang, R. Jin, Z. Shen,

Y. Wang, X. Wang, J. Xiao and X. S. Xie (2022). "BA.2.12.1, BA.4 and BA.5 escape antibodies elicited by Omicron infection." Nature **608**(7923): 593-602.

Cheng, M. H., J. M. Krieger, A. Banerjee, Y. Xiang, B. Kaynak, Y. Shi, M. Arditi and I. Bahar (2022). "Impact of new variants on SARS-CoV-2 infectivity and neutralization: A molecular assessment of the alterations in the spike-host protein interactions." iScience **25**(3): 103939.

Collaborators, C.-C. I. (2022). "Estimating global, regional, and national daily and cumulative infections with SARS-CoV-2 through Nov 14, 2021: a statistical analysis." Lancet **399**(10344): 2351-2380.

Cox, M., T. P. Peacock, W. T. Harvey, J. Hughes, D. W. Wright, C.-G. U. Consortium, B. J. Willett, E. Thomson, R. K. Gupta, S. J. Peacock, D. L. Robertson and A. M. Carabelli (2023). "SARS-CoV-2 variant evasion of monoclonal antibodies based on in vitro studies." Nat Rev Microbiol **21**(2): 112-124.

Crawford, K. H. D., R. Eguia, A. S. Dingens, A. N. Loes, K. D. Malone, C. R. Wolf, H. Y. Chu, M. A. Tortorici, D. Veesler, M. Murphy, D. Pettie, N. P. King, A. B. Balazs and J. D. Bloom (2020). "Protocol and Reagents for Pseudotyping Lentiviral Particles with SARS-CoV-2 Spike Protein for Neutralization Assays." Viruses **12**(5).

Cross, F. R., P. C. Fridy, N. E. Ketaren, F. D. Mast, S. Li, J. P. Olivier, K. Pecani, B. T. Chait, J. D. Aitchison and M. P. Rout (2023). "Expanding and improving nanobody repertoires using a yeast display method: Targeting SARS-CoV-2." J Biol Chem **299**(3): 102954.

Dadonaite, B., K. H. D. Crawford, C. E. Radford, A. G. Farrell, T. C. Yu, W. W. Hannon, P. Zhou, R. Andrabi, D. R. Burton, L. Liu, D. D. Ho, H. Y. Chu, R. A. Neher and J. D. Bloom (2023). "A pseudovirus system enables deep mutational scanning of the full SARS-CoV-2 spike." Cell **186**(6): 1263-1278 e1220.

Focosi, D., R. Quiroga, S. McConnell, M. C. Johnson and A. Casadevall (2023). "Convergent Evolution in SARS-CoV-2 Spike Creates a Variant Soup from Which New COVID-19 Waves Emerge." Int J Mol Sci **24**(3).

Fridy, P. C., Y. Li, S. Keegan, M. K. Thompson, I. Nudelman, J. F. Scheid, M. Oeffinger, M. C. Nussenzweig, D. Fenyö and B. T. Chait (2014). "A robust pipeline for rapid production of versatile nanobody repertoires." Nature methods **11**(12): 1253-1260.

Grant, O. C., D. Montgomery, K. Ito and R. J. Woods (2020). "Analysis of the SARS-CoV-2 spike protein glycan shield reveals implications for immune recognition." Sci Rep **10**(1): 14991.

Greaney, A. J., A. N. Loes, K. H. D. Crawford, T. N. Starr, K. D. Malone, H. Y. Chu and J. D. Bloom (2021). "Comprehensive mapping of mutations in the SARS-CoV-2 receptor-binding domain that affect recognition by polyclonal human plasma antibodies." Cell Host Microbe **29**(3): 463-476 e466.

Greaney, A. J., T. N. Starr, C. O. Barnes, Y. Weisblum, F. Schmidt, M. Caskey, C. Gaebler, A. Cho, M. Agudelo, S. Finkin, Z. Wang, D. Poston, F. Muecksch, T. Hatziioannou, P. D. Bieniasz, D. F. Robbiani, M. C. Nussenzweig, P. J. Bjorkman and J. D. Bloom (2021). "Mapping mutations to the SARS-CoV-2 RBD that escape binding by different classes of antibodies." Nat Commun **12**(1): 4196.

Hachmann, N. P., J. Miller, A. Y. Collier, J. D. Ventura, J. Yu, M. Rowe, E. A. Bondzie, O. Powers, N. Surve, K. Hall and D. H. Barouch (2022). "Neutralization Escape by SARS-CoV-2 Omicron Subvariants BA.2.12.1, BA.4, and BA.5." N Engl J Med **387**(1): 86-88.

Hornak, V., R. Abel, A. Okur, B. Strockbine, A. Roitberg and C. Simmerling (2006). "Comparison of multiple Amber force fields and development of improved protein backbone parameters." Proteins **65**(3): 712-725.

Imai, M., M. Ito, M. Kiso, S. Yamayoshi, R. Uraki, S. Fukushi, S. Watanabe, T. Suzuki, K. Maeda, Y. Sakai-Tagawa, K. Iwatsuki-Horimoto, P. J. Halfmann and Y. Kawaoka (2023).

"Efficacy of Antiviral Agents against Omicron Subvariants BQ.1.1 and XBB." N Engl J Med **388**(1): 89-91.

Jackson, C. B., M. Farzan, B. Chen and H. Choe (2022). "Mechanisms of SARS-CoV-2 entry into cells." Nat Rev Mol Cell Biol **23**(1): 3-20.

Jackson, L. A., E. J. Anderson, N. G. Rouphael, P. C. Roberts, M. Makhene, R. N. Coler, M. P. McCullough, J. D. Chappell, M. R. Denison, L. J. Stevens, A. J. Pruijssers, A. McDermott, B. Flach, N. A. Doria-Rose, K. S. Corbett, K. M. Morabito, S. O'Dell, S. D. Schmidt, P. A. Swanson, 2nd, M. Padilla, J. R. Mascola, K. M. Neuzil, H. Bennett, W. Sun, E. Peters, M. Makowski, J. Albert, K. Cross, W. Buchanan, R. Pikaart-Tautges, J. E. Ledgerwood, B. S. Graham, J. H. Beigel and R. N. A. S. G. m (2020). "An mRNA Vaccine against SARS-CoV-2 - Preliminary Report." N Engl J Med **383**(20): 1920-1931.

Jumper, J., R. Evans, A. Pritzel, T. Green, M. Figurnov, O. Ronneberger, K. Tunyasuvunakool, R. Bates, A. Zidek, A. Potapenko, A. Bridgland, C. Meyer, S. A. A. Kohl, A. J. Ballard, A. Cowie, B. Romera-Paredes, S. Nikolov, R. Jain, J. Adler, T. Back, S. Petersen, D. Reiman, E. Clancy, M. Zielinski, M. Steinegger, M. Pacholska, T. Berghammer, S. Bodenstein, D. Silver, O. Vinyals, A. W. Senior, K. Kavukcuoglu, P. Kohli and D. Hassabis (2021). "Highly accurate protein structure prediction with AlphaFold." Nature **596**(7873): 583-589.

Kim, S. J., J. Fernandez-Martinez, I. Nudelman, Y. Shi, W. Zhang, B. Raveh, T. Herricks, B. D. Slaughter, J. A. Hogan, P. Upla, I. E. Chemmama, R. Pellarin, I. Echeverria, M. Shivaraju, A. S. Chaudhury, J. Wang, R. Williams, J. R. Unruh, C. H. Greenberg, E. Y. Jacobs, Z. Yu, M. J. de la Cruz, R. Mironska, D. L. Stokes, J. D. Aitchison, M. F. Jarrold, J. L. Gerton, S. J. Ludtke, C. W. Akey, B. T. Chait, A. Sali and M. P. Rout (2018). "Integrative structure and functional anatomy of a nuclear pore complex." Nature **555**(7697): 475-482.

Krammer, F. (2020). "SARS-CoV-2 vaccines in development." Nature **586**(7830): 516-527.

Lan, J., J. Ge, J. Yu, S. Shan, H. Zhou, S. Fan, Q. Zhang, X. Shi, Q. Wang, L. Zhang and X. Wang (2020). "Structure of the SARS-CoV-2 spike receptor-binding domain bound to the ACE2 receptor." Nature **581**(7807): 215-220.

Laurini, E., D. Marson, S. Aulic, A. Fermeglia and S. Pricl (2021). "Molecular rationale for SARS-CoV-2 spike circulating mutations able to escape bamlanivimab and etesevimab monoclonal antibodies." Sci Rep **11**(1): 20274.

Letko, M., A. Marzi and V. Munster (2020). "Functional assessment of cell entry and receptor usage for SARS-CoV-2 and other lineage B betacoronaviruses." Nat Microbiol **5**(4): 562-569.

Li, T., W. Xue, Q. Zheng, S. Song, C. Yang, H. Xiong, S. Zhang, M. Hong, Y. Zhang, H. Yu, Y. Zhang, H. Sun, Y. Huang, T. Deng, X. Chi, J. Li, S. Wang, L. Zhou, T. Chen, Y. Wang, T. Cheng, T. Zhang, Q. Yuan, Q. Zhao, J. Zhang, J. S. McLellan, Z. H. Zhou, Z. Zhang, S. Li, Y. Gu and N. Xia (2021). "Cross-neutralizing antibodies bind a SARS-CoV-2 cryptic site and resist circulating variants." Nat Commun **12**(1): 5652.

Mannar, D., J. W. Saville, X. Zhu, S. S. Srivastava, A. M. Berezuk, K. S. Tuttle, A. C. Marquez, I. Sekirov and S. Subramaniam (2022). "SARS-CoV-2 Omicron variant: Antibody evasion and cryo-EM structure of spike protein-ACE2 complex." Science **375**(6582): 760-764.

Mast, F. D., P. C. Fridy, N. E. Ketaren, J. Wang, E. Y. Jacobs, J. P. Olivier, T. Sanyal, K. R. Molloy, F. Schmidt, M. Rutkowska, Y. Weisblum, L. M. Rich, E. R. Vanderwall, N. Dambrauskas, V. Vigdorovich, S. Keegan, J. B. Jiler, M. E. Stein, P. D. B. Olinares, L. Herlands, T. Hatziioannou, D. N. Sather, J. S. Debley, D. Fenyo, A. Sali, P. D. Bieniasz, J. D. Aitchison, B. T. Chait and M. P. Rout (2021). "Highly synergistic combinations of nanobodies that target SARS-CoV-2 and are resistant to escape." Elife **10**.

McCallum, M., A. De Marco, F. A. Lempp, M. A. Tortorici, D. Pinto, A. C. Walls, M. Beltramello, A. Chen, Z. Liu, F. Zatta, S. Zepeda, J. di Iulio, J. E. Bowen, M. Montiel-Ruiz, J. Zhou, L. E. Rosen, S. Bianchi, B. Guarino, C. S. Fregni, R. Abdelnabi, S. C. Foo, P. W. Rothlauf, L. M. Bloyet, F. Benigni, E. Cameroni, J. Neyts, A. Riva, G. Snell, A. Telenti, S. P. J. Whelan, H. W. Virgin, D. Corti, M. S. Pizzuto and D. Veesler (2021). "N-terminal domain antigenic mapping reveals a site of vulnerability for SARS-CoV-2." Cell **184**(9): 2332-2347 e2316.

Mendoza, E. J., K. Manguiat, H. Wood and M. Drebot (2020). "Two Detailed Plaque Assay Protocols for the Quantification of Infectious SARS-CoV-2." Curr Protoc Microbiol **57**(1): ecpmc105.

Meng, Y., D. M. Irwin and Y. Shen (2023). "Ecology of SARS-CoV-2 in the post-pandemic era." Lancet Microbe **4**(4): e208.

Mirdita, M., K. Schutze, Y. Moriwaki, L. Heo, S. Ovchinnikov and M. Steinegger (2022). "ColabFold: making protein folding accessible to all." Nat Methods **19**(6): 679-682.

Motozono, C., M. Toyoda, J. Zahradnik, A. Saito, H. Nasser, T. S. Tan, I. Ngare, I. Kimura, K. Uriu, Y. Kosugi, Y. Yue, R. Shimizu, J. Ito, S. Torii, A. Yonekawa, N. Shimono, Y. Nagasaki, R. Minami, T. Toya, N. Sekiya, T. Fukuhara, Y. Matsuura, G. Schreiber, C. Genotype to Phenotype Japan, T. Ikeda, S. Nakagawa, T. Ueno and K. Sato (2021). "SARS-CoV-2 spike L452R variant evades cellular immunity and increases infectivity." Cell Host Microbe **29**(7): 1124-1136 e1111.

Muyldermans, S. (2013). "Nanobodies: natural single-domain antibodies." Annu Rev Biochem **82**: 775-797.

Pettersen, E. F., T. D. Goddard, C. C. Huang, E. C. Meng, G. S. Couch, T. I. Croll, J. H. Morris and T. E. Ferrin (2021). "UCSF ChimeraX: Structure visualization for researchers, educators, and developers." Protein Sci **30**(1): 70-82.

Pilz, S. and J. P. A. Ioannidis (2023). "Does natural and hybrid immunity obviate the need for frequent vaccine boosters against SARS-CoV-2 in the endemic phase?" Eur J Clin Invest **53**(2): e13906.

Planas, D., D. Veyer, A. Baidaliuk, I. Staropoli, F. Guivel-Benhassine, M. M. Rajah, C. Planchais, F. Porrot, N. Robillard, J. Puech, M. Prot, F. Gallais, P. Gantner, A. Velay, J. Le Guen, N. Kassis-Chikhani, D. Edriss, L. Belec, A. Seve, L. Courtellemont, H. Pere, L. Hocqueloux, S. Fafi-Kremer, T. Prazuck, H. Mouquet, T. Bruel, E. Simon-Loriere, F. A. Rey and O. Schwartz (2021). "Reduced sensitivity of SARS-CoV-2 variant Delta to antibody neutralization." Nature **596**(7871): 276-280.

Polack, F. P., S. J. Thomas, N. Kitchin, J. Absalon, A. Gurtman, S. Lockhart, J. L. Perez, G. Perez Marc, E. D. Moreira, C. Zerbini, R. Bailey, K. A. Swanson, S. Roychoudhury, K. Koury, P. Li, W. V. Kalina, D. Cooper, R. W. Frenck, Jr., L. L. Hammitt, O. Tureci, H. Nell, A. Schaefer, S. Unal, D. B. Tresnan, S. Mather, P. R. Dormitzer, U. Sahin, K. U. Jansen, W. C. Gruber and C. C. T. Group (2020). "Safety and Efficacy of the BNT162b2 mRNA Covid-19 Vaccine." N Engl J Med **383**(27): 2603-2615.

Rausch, R. (1991). "Effects of temporal lobe surgery on behavior." Adv Neurol **55**: 279-292.

Rodrigues, J. P., M. Trellet, C. Schmitz, P. Kastritis, E. Karaca, A. S. Melquiond and A. M. Bonvin (2012). "Clustering biomolecular complexes by residue contacts similarity." Proteins **80**(7): 1810-1817.

Rout, M. P. and A. Sali (2019). "Principles for Integrative Structural Biology Studies." Cell **177**(6): 1384-1403.

Sali, A. (2021). "From integrative structural biology to cell biology." Journal of Biological Chemistry **296**.

Saltzberg, D. J., S. Viswanath, I. Echeverria, I. E. Chemmama, B. Webb and A. Sali (2021). "Using Integrative Modeling Platform to compute, validate, and archive a model of a protein complex structure." Protein Sci **30**(1): 250-261.

Starr, T. N., A. J. Greaney, A. Addetia, W. W. Hannon, M. C. Choudhary, A. S. Dingens, J. Z. Li and J. D. Bloom (2021). "Prospective mapping of viral mutations that escape antibodies used to treat COVID-19." Science **371**(6531): 850-854.

Starr, T. N., A. J. Greaney, A. S. Dingens and J. D. Bloom (2021). "Complete map of SARS-CoV-2 RBD mutations that escape the monoclonal antibody LY-CoV555 and its cocktail with LY-CoV016." Cell Rep Med **2**(4): 100255.

Starr, T. N., A. J. Greaney, W. W. Hannon, A. N. Loes, K. Hauser, J. R. Dillen, E. Ferri, A. G. Farrell, B. Dadonaite, M. McCallum, K. A. Matreyek, D. Corti, D. Veesler, G. Snell and J. D. Bloom (2022). "Shifting mutational constraints in the SARS-CoV-2 receptor-binding domain during viral evolution." Science **377**(6604): 420-424.

Takashita, E., S. Yamayoshi, V. Simon, H. van Bakel, E. M. Sordillo, A. Pekosz, S. Fukushi, T. Suzuki, K. Maeda, P. Halfmann, Y. Sakai-Tagawa, M. Ito, S. Watanabe, M. Imai, H. Hasegawa and Y. Kawaoka (2022). "Efficacy of Antibodies and Antiviral Drugs against Omicron BA.2.12.1, BA.4, and BA.5 Subvariants." N Engl J Med **387**(5): 468-470.

Tegally, H., M. Moir, J. Everatt, M. Giovanetti, C. Scheepers, E. Wilkinson, K. Subramoney, Z. Makatini, S. Moyo, D. G. Amoako, C. Baxter, C. L. Althaus, U. J. Anyaneji, D. Kekana, R. Viana, J. Giandhari, R. J. Lessells, T. Maponga, D. Maruapula, W. Choga, M. Matshaba, M. B. Mbulawa, N. Msomi, N.-S. consortium, Y. Naidoo, S. Pillay, T. J. Sanko, J. E. San, L. Scott, L. Singh, N. A. Magini, P. Smith-Lawrence, W. Stevens, G. Dor, D. Tshiabuila, N. Wolter, W. Preiser, F. K. Treurnicht, M. Venter, G. Chiloane, C. McIntyre, A. O'Toole, C. Ruis, T. P. Peacock, C. Roemer, S. L. Kosakovsky Pond, C. Williamson, O. G. Pybus, J. N. Bhiman, A. Glass, D. P. Martin, B. Jackson, A. Rambaut, O. Laguda-Akingba, S. Gaseitsiwe, A. von Gottberg and T. de Oliveira (2022). "Emergence of SARS-CoV-2 Omicron lineages BA.4 and BA.5 in South Africa." Nat Med **28**(9): 1785-1790.

Twarog, N. R., E. Stewart, C. V. Hammill and A. A. Shelat (2016). "BRAID: A Unifying Paradigm for the Analysis of Combined Drug Action." Sci Rep **6**: 25523.

Walls, A. C., Y. J. Park, M. A. Tortorici, A. Wall, A. T. McGuire and D. Veesler (2020). "Structure, Function, and Antigenicity of the SARS-CoV-2 Spike Glycoprotein." Cell **181**(2): 281-292 e286.

Wang, F., L. Li, Y. Dou, R. Shi, X. Duan, H. Liu, J. Zhang, D. Liu, J. Wu, Y. He, J. Lan, B. Lu, H. Feng and J. Yan (2022). "Etesevimab in combination with JS026 neutralizing SARS-CoV-2 and its variants." Emerg Microbes Infect **11**(1): 548-551.

Wang, Q., Y. Guo, S. Iketani, M. S. Nair, Z. Li, H. Mohri, M. Wang, J. Yu, A. D. Bowen, J. Y. Chang, J. G. Shah, N. Nguyen, Z. Chen, K. Meyers, M. T. Yin, M. E. Sobieszczyk, Z. Sheng, Y. Huang, L. Liu and D. D. Ho (2022). "Antibody evasion by SARS-CoV-2 Omicron subvariants BA.2.12.1, BA.4 and BA.5." Nature **608**(7923): 603-608.

Wang, Y., C. Liu, C. Zhang, Y. Wang, Q. Hong, S. Xu, Z. Li, Y. Yang, Z. Huang and Y. Cong (2022). "Structural basis for SARS-CoV-2 Delta variant recognition of ACE2 receptor and broadly neutralizing antibodies." Nat Commun **13**(1): 871.

Wang, Z., F. Muecksch, A. Cho, C. Gaebler, H. H. Hoffmann, V. Ramos, S. Zong, M. Cipolla, B. Johnson, F. Schmidt, J. DaSilva, E. Bednarski, T. B. Tanfous, R. Raspe, K. Yao, Y. E. Lee, T. Chen, M. Turroja, K. G. Milard, J. Dizon, A. Kaczynska, A. Gazumyan, T. Y. Oliveira, C. M. Rice, M. Caskey, P. D. Bieniasz, T. Hatziioannou, C. O. Barnes and M. C. Nussenzweig (2022). "Conserved Neutralizing Epitopes on the N-Terminal Domain of Variant SARS-CoV-2 Spike Proteins." bioRxiv.

Watanabe, Y., J. D. Allen, D. Wrapp, J. S. McLellan and M. Crispin (2020). "Site-specific glycan analysis of the SARS-CoV-2 spike." Science **369**(6501): 330-333.

Webb, B., S. Viswanath, M. Bonomi, R. Pellarin, C. H. Greenberg, D. Saltzberg and A. Sali (2018). "Integrative structure modeling with the Integrative Modeling Platform." Protein Sci **27**(1): 245-258.

Wec, A. Z., D. Wrapp, A. S. Herbert, D. P. Maurer, D. Haslwanter, M. Sakharkar, R. K. Jangra, M. E. Dieterle, A. Lilov, D. Huang, L. V. Tse, N. V. Johnson, C. L. Hsieh, N. Wang, J. H. Nett, E. Champney, I. Burnina, M. Brown, S. Lin, M. Sinclair, C. Johnson, S. Pudi, R. Bortz, 3rd, A. S. Wirchnianski, E. Laudermilch, C. Florez, J. M. Fels, C. M. O'Brien, B. S. Graham, D. Nemazee, D. R. Burton, R. S. Baric, J. E. Voss, K. Chandran, J. M. Dye, J. S. McLellan and L. M. Walker (2020). "Broad neutralization of SARS-related viruses by human monoclonal antibodies." Science **369**(6504): 731-736.

Wooten, D. J. and R. Albert (2021). "synergy: a Python library for calculating, analyzing and visualizing drug combination synergy." Bioinformatics **37**(10): 1473-1474.

Wrapp, D., D. De Vlieger, K. S. Corbett, G. M. Torres, W. Van Breedam, K. Roose, L. van Schie, V.-C. COVID, R. Team and M. Hoffmann (2020). "Structural basis for potent neutralization of betacoronaviruses by single-domain camelid antibodies (preprint)."

Yan, Q., R. Hou, X. Huang, Y. Zhang, P. He, Y. Zhang, B. Liu, Q. Wang, H. Rao, X. Chen, X. Zhao, X. Niu, J. Zhao, X. Xiong and L. Chen (2022). "Shared IGHV1-69-encoded neutralizing antibodies contribute to the emergence of L452R substitution in SARS-CoV-2 variants." Emerg Microbes Infect **11**(1): 2749-2761.

Zhang, J., T. Xiao, Y. Cai, C. L. Lavine, H. Peng, H. Zhu, K. Anand, P. Tong, A. Gautam, M. L. Mayer, R. M. Walsh, Jr., S. Rits-Volloch, D. R. Wesemann, W. Yang, M. S. Seaman, J. Lu and B. Chen (2021). "Membrane fusion and immune evasion by the spike protein of SARS-CoV-2 Delta variant." Science **374**(6573): 1353-1360.

Zhao, P., J. L. Praissman, O. C. Grant, Y. Cai, T. Xiao, K. E. Rosenbalm, K. Aoki, B. P. Kellman, R. Bridger, D. H. Barouch, M. A. Brindley, N. E. Lewis, M. Tiemeyer, B. Chen, R. J. Woods and L. Wells (2020). "Virus-Receptor Interactions of Glycosylated SARS-CoV-2 Spike and Human ACE2 Receptor." Cell Host Microbe **28**(4): 586-601 e586.

Zhao, Z., J. Zhou, M. Tian, M. Huang, S. Liu, Y. Xie, P. Han, C. Bai, P. Han, A. Zheng, L. Fu, Y. Gao, Q. Peng, Y. Li, Y. Chai, Z. Zhang, X. Zhao, H. Song, J. Qi, Q. Wang, P. Wang and G. F. Gao (2022). "Omicron SARS-CoV-2 mutations stabilize spike up-RBD conformation and lead to a non-RBM-binding monoclonal antibody escape." Nat Commun **13**(1): 4958.

SUPPLEMENTAL MATERIAL

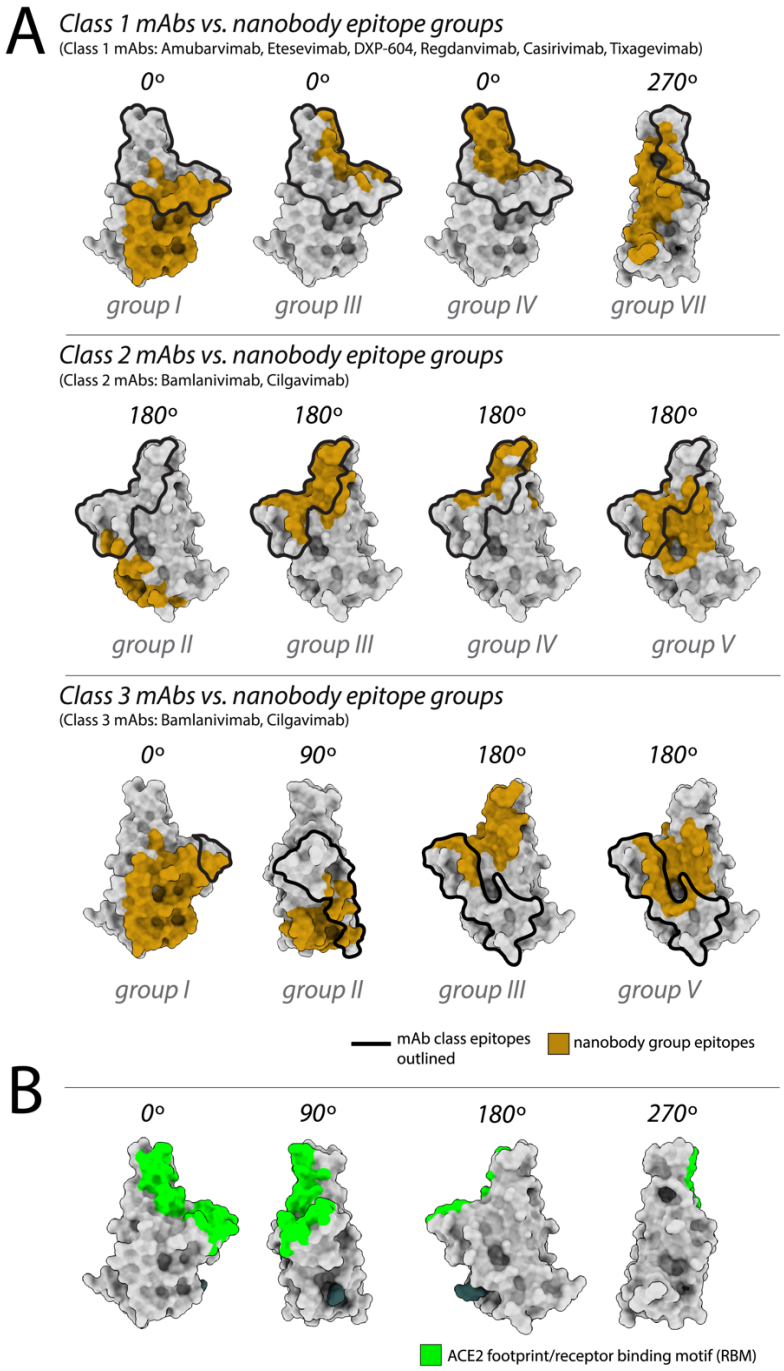

Supplementary Figure 1. (A) Nanobody epitope groups overlapping with the three mAb epitope classes (class 1, class 2 and class 3). Nanobody groups are colored in gold and mAb class footprints are outlined in black. mAb epitopes are taken from Cox et al (Cox, Peacock et al.). (**B**) A single RBD subunit with the ACE2 footprint/RBM mapped

in green. All epitopes are mapped on the structure of the RBD (PDB ID: 6M0J). All structure representations were created on ChimeraX (Pettersen, Goddard et al.).

Supplementary Table 1 - Neutralization data from synergy experiments